Hindawi Publishing Corporation
International Journal of Distributed Sensor Networks
Volume 2012, Article ID 785418, 12 pages
doi:10.1155/2012/785418

Research Article

Hybrid BS-Cooperative Power Management Scheme with Self-Organized Sleep Mode in Virtual Cell-Based Femto Networks

Wei Zheng,[1,2] Wei Li,[1,2] Yuanbao Xie,[1,2] and Xiangming Wen[1,2]

[1] *School of Information and Communication Engineering, Beijing University of Posts and Telecommunications, Beijing 100876, China*
[2] *Beijing Key Lab of Network System Architecture and Convergence, Beijing University of Posts and Telecommunications, Beijing 100876, China*

Correspondence should be addressed to Wei Zheng, zhengweius@gmail.com

Received 4 May 2012; Revised 19 September 2012; Accepted 21 September 2012

Academic Editor: Yiqing Zhou

A large-scale deployment of femtocell BSs (FBSs) causes substantial energy consumption. This paper proposes a hybrid BS-cooperative power management (HBCPM) scheme with self-organized sleep mode in virtual cell-based femto networks. Firstly, HBCPM builds a leader-member virtual cell framework, in which only one FBS is a FBS leader (FL) and others are FBS members (FMs). Then, the FL acts as an autonomous entity and is responsible for detecting active calls in the virtual cell coverage, while the FMs without active connections can entirely shut down pilot transmissions and the related processing all the time. So it is suited for self-organizing networks (SONs). Based on the proposed scheme, the state transition model is established by the semi-Markov stochastic process, and the analytic formulas of average cumulative delay and interference time as well as the energy consumption are derived. Meanwhile, three prominent-related schemes are also studied by the proposed model. With the practical long-term evolution (LTE) system parameters and three-dimensional femtocell network model, the numerical simulation and theoretical analysis match pretty well, and the tradeoff between the energy consumption and average cumulative delay is also manifested. Moreover, simulation results show that the proposed algorithm outperforms other three schemes in terms of average cumulative interference time and the energy consumption.

1. Introduction

1.1. The Motivation. The tremendous success of mobile cellular networks leads to wide proliferation and demand for ubiquitous heterogeneous broadband mobile wireless services, meanwhile, recent investigation confirms that most of voice services and data services take place in indoor scenarios [1]. Due to the high penetration loss and the long transmission distance, there is a huge cost for the macrocell to serve massive indoor users with extensive transmission demands. To address this problem, the applications of so called femtocell BS (FBS) have been investigated [1]. FBS is a short-range, low-power, low-cost, as well as customer-owned cellular base station deployed by the terminal consumers. It is connected to the existing broadband access network via fixed backhaul such as digital subscriber line or coaxial cable. FBS brings with it not only the enhanced indoor coverage without much additional cost, but also the other significant benefits such as increased spectral efficiency, offloaded macrocell burden, improved network capacity, and prolonged life for phone battery.

Although femtocell technique is deemed to be an emerging candidate solution of catering for the ever-growing demand for the wireless service, researchers and operators so far mainly focused on capacity or spectrum efficiency improvement by adding the femtocell into the macrocell [2–4] and do not pay much enough attention to the potential energy expenditure with more FBSs. ABI research [5] predicts that more than 36 million of femtocells are expected to be sold worldwide with 150 million of customers by the end of year 2012, and thus the energy consumption of the wireless cellular network might be drastically increased by the overwhelming FBSs. The growth of the energy consumption will cause an increase in global carbon dioxide emissions and impose more and more challenging operational costs for operators. Therefore, it is necessary to consider the energy

consumption of femtocell networks, and then design an energy saving scheme without sacrificing its core benefits and functions.

Contrasting with macrocells, the traffic load of femtocell networks has more significant fluctuations in space and time due to a number of factors such as user mobility and behavior, as well as supporting very fewer simultaneous users for each FBS. During daytime, traffic load is generally higher in office areas compared to residential areas, while it is the other way around during the night. Therefore, there will always be some femtocells under the low traffic load, while some others may be under the heavy traffic load. However, FBSs in current cellular network architecture are always required to be active on air interface by continuously transmitting pilot signals and doing some related processing. In addition, the wireless air interface consumes energy with the same rate in receive, transmit, or idle states. In turn, the less the wireless air interface is operating, the less energy is consumed as well as the fewer interference time is caused. Hence, the most important issue in developing networks which are energy-aware is to model the power consumption of the wireless air interface [6]. So, energy saving potential of FBSs needs to be exploited by designing protocols to enable to shut down the wireless air interface, or to go to the sleep mode in FBSs [6]. Then, it is also necessary to study a suitable scheme to control the sleep mode behavior for FBSs.

1.2. Related Work. With green communication emerging, energy efficiency has become an important system design parameter for the long-term economic evaluation indicator of cellular networks. Researchers and operators gradually focus on the energy efficiency in two-tier femtocell networks [7–9]. Khirallah and Thompson present a methodology for estimating the total energy consumption, taking into account the total operational power and embodied energy, and TCO (total-cost-of-ownership) of two-tier femtocell cellular networks [7], which also shows that macro-femtocell networks reduce the networks TCO at the expense of increased energy-consumption. The above study mainly analyze energy efficiency whether can be improved with the femtocell deployment. However, they do not consider how to reduce energy consumption for a large-scale deployment of femtocells. Cheng et al. [8] introduce a spectrum splitting strategy to minimize the downlink energy consumption while suppress cross-tier interference. Domenico et al. [9] propose two resource management schemes that can limit the overall interference per resource block (RB) from neighbor FBSs and reduce the transmission power in each RB as well.

Usually, the wireless interface consumes energy with the same rate in receive, transmit, or idle states. In turn, the less the wireless interface is operating, the less energy is consumed. Therefore, the best strategy to minimize the energy consumption is to shut down the wireless interface, or to go to energy saving mode [6]. By contrast, there are relative less literature on designing protocols to enable sleep modes in FBSs and controlling the sleep mode behavior of FBSs for energy efficient improvement. The LTE standard introduces power saving protocols such as discontinuous transmission (DTX) and discontinuous reception (DRX) mode for both mobile stations and base stations [10]. DTX and DRX are methods to momentarily power down the device by switching off the transceivers whenever there is no need to transmit or receive. A timer-based energy-efficient solution is presented in IEEE 802.16 m standard [11] that the FBS periodically transmits pilot signals in low traffic scenario. The transmission period of the pilot signal is divided into two parts: fixed available and unavailable intervals, where the FBS switches off pilot transmissions and enters into the sleep mode. To reduce unnecessary available intervals, Widiarti et al. propose a dynamic shutting down pilot transmissions mechanism based on FBSs grouping [12]. However, the above schemes will not be efficient as long as the sleep/idle users are in the FBS coverage. Regarding this, the FBS does not need to turn on its pilot transmissions and related processing via user activity detection, irrespective of the location of registered users [13]. Nevertheless, this scheme only studies how to reduce the energy consumption from single FBS aspect, not suitable for the large-scale femtocell deployments. It also does not analyze the impact of various key parameters on the proposed scheme such as session arrival rate and so on.

1.3. The Contributions. In this paper, a novel hybrid (centralized/distributed) BS-cooperative power management (HBCPM) scheme is proposed for self-organized sleep mode in virtual cell-based femto networks. Firstly, according to the femtocell network topology, BCHPM builds a leader-member virtual cell framework, that is, femtocell networks are classified into a number of virtual cells based on one-hop neighbor list, the size of which is the sum of the sizes of FBSs. Within each virtual cell, the FBS is elected as either a FBS leader (FL) or a FBS member (FM) based on the list degree and the sum of received pilot signal power. Moreover, because of the time variation characteristic of the femtocell network topology, the role assignment algorithm for the newly installed FBS is introduced. Secondly, the FL is responsible for detecting active calls in the virtual cell coverage, while the FMs without the active user can completely switch off the pilot transmission and the associated processing all the time. Once the active registered user is detected by the FL, FL cooperates with the target FM, and then the target FM becomes active on the wireless air interface. Thirdly, the performance of HBCPM is analyzed theoretically in terms of average cumulative delay and the energy consumption and average cumulative interference time from the following two aspects: (i) state transition model is established; (ii) the analytic formulas of average cumulative delay and interference time and the energy consumption are derived. Finally, according to theoretical analysis of the proposed scheme, we further research three-prominent related schemes, and then, we assess the effectiveness of the proposed scheme by comparing its performance with them. With a three dimensional (3D) femtocell network model and practical LTE parameters, simulation results show that the proposed scheme outperforms three existing schemes in terms of average accumulative interference time and the energy consumption. Furthermore, the results provide some guidelines for deploying energy efficient femtocell networks.

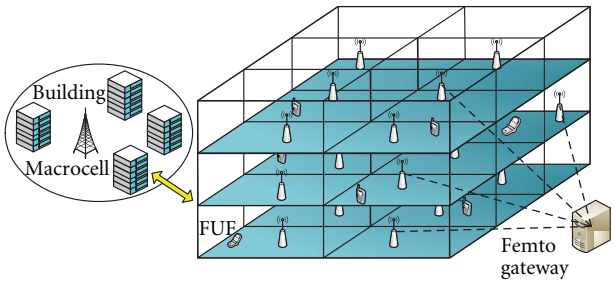

Figure 1: The two-tier femtocell cellular network deployment.

The rest of this paper is organized as follows. Section 2 presents a 3D femtocell network deployment model, and describes a novel hybrid BS-cooperative power management scheme for the self-organized sleep mode in virtual cell-based femto networks. Section 3 analyzes the proposed scheme theoretically from the aspects of the energy saving and average cumulative delay and interference time. Meanwhile, three-prominent related schemes are investigated in theory as well. Section 4 provides simulation results and discussions. Finally, Section 5 concludes the paper and future work.

2. Approach: HBCPM

2.1. Femtocell Cellular Network Model. Figure 1 shows three dimensional topology of two-tier femtocell cellular networks, also called macrocell-femtocell overlay networks. A large number of FBSs with a small coverage area are randomly distributed on every floor of office blocks or residential buildings. The buildings are in the coverage of single overlay macrocell BS (MBS), and all FBSs in the building are under the centralized control of a femtocell server referred as the femto gateway (F-GW), which manages operation and maintenance (OAM) information such as the femtocell location and the identification through a backhaul link [14]. In addition, closed subscriber group (CSG) mode is adopted in this paper, where only authorized users and a list of invited users are allowed to access the given femtocell and occupy the resources for data communications.

2.2. Proposed Scheme. This section presents the HBCPM approach, which is based on the following two main components: (i) leader-member virtual cell construction, (ii) hybrid FBS-cooperative power management.

2.2.1. Leader-Member Virtual Cell Construction. The objective of this part is to describe the virtual cell construction procedure which divides the femtocell network into different virtual cells. Considering the uneven distribution of the FBSs in femtocell networks, a virtual cell construction algorithm is proposed on the basis of the femtocell distribution density and the received pilot signal power strength. According to the third generation partnership project (3GPP) standard [15], when a FBS is installed or switched on, it firstly enters into an initialization state. The FBS in this state needs to scan the radio environment to search for neighbor FBSs for getting necessary information. During this scanning process, the one-hop neighbor list including the received pilot signal power indicator from neighbors can be obtained. Note that the received pilot signal power strength must be above the predefined threshold to ensure that they are very close.

Utilizing the one-hop list, each FBS can calculate the sum of the received pilot signal power and the number of the FBSs in the list (i.e., list degree), and then sends these information to the F-GW. Note that the greater the sum of the received pilot energy strength or the list degree is, the more FBSs are located around this FBS. In subsequent frame, the F-GW elects the one which has the highest list degree among all FBSs as the first FL. If more than one FBSs are chosen as the FLs, the one with the maximal is chosen as the first FL. If the sums of the received pilot signal power are equal, break the tie randomly. After the first FL is determined, each FBS in the first FL's one-hop list decides whether it can be a FM of the first FL. If one FBS calculates that the pilot signal power received from the first FL is maximal in its one-hop list, it serves as FMs and attached to the elected FL. Otherwise, wait for the next role assignment. After the first virtual cell is generated, the second virtual cell is initiated with the FBS having the highest sum of the received pilot signal power among FBSs excluding the ones belonging to the first virtual cell and is updated as the first virtual cell. Besides, the rest of virtual cells are also constructed in the same way.

More formally, the whole algorithm to construct the virtual cell is summarized in Algorithm 1, where the set of operational FBSs in the femtocell network is given by $\varphi = \{1, 2, \ldots, N\}$. ψ_n is the set of FBSs which are in the one-hop list of the FBS n, and $|\psi_n|$ denotes the list degree of the FBS n. Define the received pilot signal power measured by the FBS n, from the FBS m as p_{nm} $(n, m \in \varphi)$, and p_n represents the sum of the received pilot signal power computed by the FBS n.

Furthermore, a role assignment algorithm is studied for the newly added FBS. When the new FBS F_n is installed, it scans the surrounding area to search for neighbor FBSs and sends the one-hop list to the F-GW. Since the F-GW has the global knowledge about the topology of the femtocell networks, it knows each virtual cell configuration, including the FL and the FMs based on the identification. Then, using this information, the F-GW will send a message to notify the new FBS what role it should play. If there is only one FL in the one-hop list, the new FBS serves as a FM belonging to this FL; if there are more than one FLs in the list, compare the pilot power received from these FLs and choose the one with the largest pilot power as the FL of the new FBS (if the received pilot power is equal, break the tie randomly). Otherwise, the new FBS forms a new virtual cell by itself and be a FL. The role assignment algorithm for the new FBS is described by the pseudocode in Algorithm 2.

2.2.2. Hybrid FBS-Cooperative Power Management. The object of this part is to present the FBS-cooperative power management algorithm in each virtual cell. We need to introduce a low power consumption device installed with each FBS, called a sniffer. It is used to detect the energy strength of

Initialize: $p_n = 0$, $p_{nm} = 0$, $\psi_n = \phi$, $\varphi = \{1, 2, \ldots, N\}$, $|\psi_n| = 0$, $n, m = 1, 2, \ldots, N$
(1) Each FBS n creates the one-hop list and calculates the list degrees $|\psi_n|$ and the sum of the received pilot signal power $p_n = \sum_{m \in \psi_n} p_{nm}$;
(2) Elect the FL n^* from set φ, where $n^* = \arg_{n \in \varphi} \max |\psi_n|$. If there is more than one maximum, choose the FBS n^{**} as the FL, where $n^{**} = \arg_{n^*} \max p_n$. If sums of the pilot signal power are equal, break the tie randomly;
(3) Update the lth virtual cell as $C_l = \{n^{**}\}$;
(4) If $\psi_{n^{**}} \neq \phi$, the FBS $m^* \in \psi_{n^{**}} \cap \varphi$ acts as a FM of the lth virtual cell, which should meet the following condition: $p_{m^* n^{**}} \geq p_{m^* n'}, \forall n' \in \psi_{m^*}$; otherwise go to step 6;
(5) update C_l as: $C_l \leftarrow C_l \cup \{m^* \mid p_{m^* n^{**}} \geq p_{m^* n'}, \forall n' \in \psi_{m^*}\}$;
(6) Update φ to exclude the FBSs belonging to the first virtual cell, that is, $\varphi \leftarrow \varphi \setminus C_l$, and then recalculate $|\psi_n|$ and p_n, $(n \in \varphi)$;
(7) Repeat steps 2~6 until the set φ is empty.

Algorithm 1: Virtual cell construction algorithm.

(1) F_n scans the surrounding radio environments and creates the one-hop neighbor list;
(2) F_n sends the one-hop list to the F-GW, and then the F-GW notifies F_n what role it should serve as;
(3) **if** F_n has only one FL in its one-hop neighbor list, **then**
(4) the F-GW elects this FBS as the FL of F_n, and F_n acts as a FM;
(5) **else**
(6) **if** F_n has more than one FLs in its one-hop list, **then**
(7) compare the pilot power strength of F_n received from these FLs, and choose the one with the largest pilot power strength as the FL of F_n;
(8) **else**
(9) F_n forms a new virtual cell by itself and be a FL
(10) **end if**
(11) **end if**

Algorithm 2: Role assignment algorithm.

an active call. In each virtual cell, the sniffer of the FL needs to keep alive all the time. When there is an active call in the virtual cell coverage, the sniffer of FL detects an energy rise of the received signal on the uplink frequency band. If the received signal energy strength is higher than the predefined threshold, the registered user with an active call is considered to be close enough to the virtual cell.

Figure 2 shows the operational flowchart of cooperative FBS power management procedure. Assume that the FL can exchange information with the FMs in the same virtual cell, similar to the information interaction among MBSs through X2 interface in 3GPP [14]. Take a virtual cell for example. In the initial state, the FBSs without the active user in the virtual cell disable pilot transmissions and the associated processing and the sniffers, while the sniffer of the FL is busy performing measurements on the macrocell uplink band. When the sniffer of the FL detects an active registered user in the vicinity of the virtual cell and the received energy strength p_{MF} exceeds the threshold level p_{TH}^1, the FL sends a message to notify the target FM to open the sniffer. Here, we assume that the FL knows which FM the registered user can access. Meanwhile, the time counter of the target FM is started and the sniffer begins to detect the energy rise in the received signal. If the received energy strength is lower than the threshold p_{TH}^2 within the timer range T_0, the sniffer switches off and the time counter resets immediately, then the target FBS returns to the origin state and sends message to the FL. Otherwise, the target FM switches on pilot transmissions and the associated processing. Then, the registered user can detect the target FM in the next scanning and establish a connection with it. After the active call is finished, the target FM turns off the pilot transmission and the processing and sends message to notify the FL.

Specially, when the sniffer of the FL detects the registered user making an active call in the target FM coverage area, the FL directly notifies the target FM to activate the sniffer and pilot transmissions. By doing so, the active user can detect the target FM and perform handover to it with a slight delay.

3. Theoretical Analysis

This section establishes a state transition model based on the proposed scheme, and then closed form expressions of the energy consumption, average cumulative delay, and interference time are derived.

3.1. State Transition Model. To analyze the proposed scheme, we build up the state transition model including the following three states as shown in Figure 3. For the ease of description, define these states as state 1, state 2, and state 3, respectively. In each state, the FL needs to keep its sniffer on for the active call detection. In state 1, not only the pilot

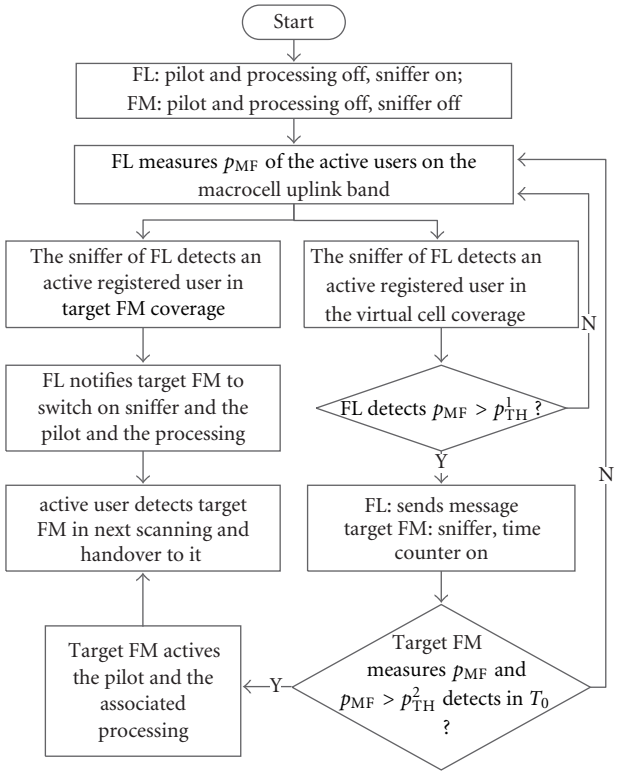

Figure 2: Flowchart of hybrid FBS-Cooperative Power Management.

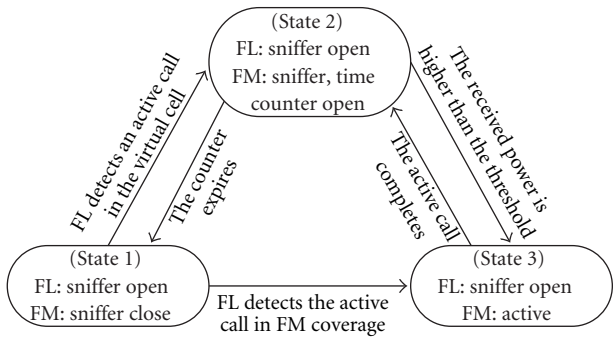

Figure 3: State transition model for HBCPM.

transmission and the associated processing of the FMs are off, but also the sniffer. When the sniffer of the FL detects an active registered user in the vicinity of the virtual cell and the received signal energy strength exceeds the threshold level, the FM moves into state 2. In state 2, both the sniffer and the time counter of the FM are on. If there is no session arrival in the timer range, the time counter is reset and the sniffer is switched off immediately, and the FM returns back to the state 1. Otherwise, the FM enters into the state 3. In state 3, the pilot transmission and the processing of the FM are both on, which provides services with active users. If the active call completes, the FM disables its pilot transmission and moves into state 2. Specially, when the sniffer of the FL detects an active registered user in the target FM coverage, the target FM directly enters into state 3.

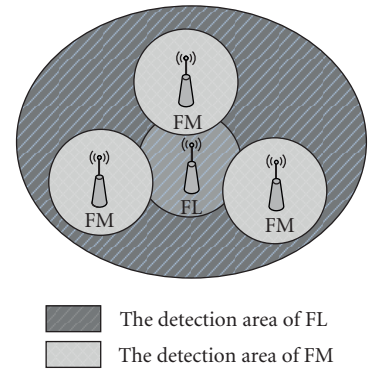

Figure 4: simplified model of femtocell deployments.

3.2. Analysis of the Proposed Scheme. Our objective in this subsection is to derive the analytic formulas of the energy consumption, average cumulative delay, and interference time. For simplicity, we consider a single virtual cell which consists of a FL and a FM as illustrated in Figure 4. The detection area of the FL is the coverage of the virtual cell, while the detection area of the FM is its own coverage. First, we shall make the following assumptions for the rest of the work.

AS 1. At the initial condition, no user exists in the FM coverage or the users under the coverage of the FM are in sleep/idle mode.

AS 2. The session arrival in the virtual cell coverage and the FM coverage follow Poisson distribution with the rate λ_c and λ_m, respectively.

AS 3. The time duration in state 1 follows a $M/M/\infty$ queuing model, and the service time for each session follows negative exponential distribution with the average service rate ρ, ($\rho > 0$).

AS 4. The timer range of the time counter of the FBS is constant and set as T_0.

Let the waiting time of the nth session arrival be defined as T_n. Based on the assumption above, the distribution function $M_{T_n}(t)$ and probability density function $m_{T_n}(t)$ of T_n can be given by

$$M_{T_n}(t) = P(T_n \le t) = 1 - e^{-\lambda_m t}, \quad t > 0,$$
$$m_{T_n}(t) = \frac{dM_{T_n}(t)}{dt} = \lambda_m e^{-\lambda_m t}, \quad t > 0. \tag{1}$$

According to the state transition model, define the energy consumption E of the FBS per hour, average cumulative delay D_{ave}, and interference time T_{int}, respectively, as

$$\begin{aligned} E &= \sum_{i=1}^{3} E_i P_i, \quad i = 1,2,3, \\ D_{\text{ave}} &= \frac{P_1 \times \overline{t_1} \times \lambda_m \times (D_{12} + D_{23}) + P_2 \times \overline{t_2} \times \lambda_m \times D_{23}}{(P_1 \times \overline{t_1} + P_2 \times \overline{t_2} + P_3 \times \overline{t_3}) \times \lambda_m} \\ &= \frac{P_1 \times \overline{t_1} \times (D_{12} + D_{23}) + P_2 \times \overline{t_2} \times D_{23}}{P_1 \times \overline{t_1} + P_2 \times \overline{t_2} + P_3 \times \overline{t_3}}, \\ T_{\text{int}} &= P_3 T_H, \end{aligned} \tag{2}$$

where E_i denotes the energy consumption of the FBS per hour in state i and P_i represents the steady state probability of each state. $\overline{t_i}$ is the mean residence time of the FBS in state i. D_{12} and D_{23} are average cumulative delay needed to initiate a new session from state 1 to state 2 and from state 2 to state 3, respectively. T_H is a statistical period. Since the residence time of the FBS in each state does not follow the exponential distribution, a semi-Markov process model is introduced to analyze the state transition behavior of the FBS [16]. Thus, the steady state probability of each state can be represented as

$$P_i = \frac{\pi_i \overline{t_i}}{\sum_{j=1}^{3} \pi_j \overline{t_j}}, \quad i = 1,2,3, \tag{3}$$

where π_i represents the stationary probability of the state i, which can be obtained by solving the following equations:

$$\begin{aligned} \pi_i &= \sum_{j=1}^{3} \pi_j P_{ij}, \quad j = 1,2,3, \\ 1 &= \sum_{j=1}^{3} \pi_j, \end{aligned} \tag{4}$$

where P_{ij} is the transition probability from the state i to the state j. According to the state transition model, the state transition probability matrix H can be directly given by

$$H = \left(P_{ij}\right) = \begin{pmatrix} 0 & P_{12} & P_{13} \\ P_{21} & 0 & P_{23} \\ 0 & P_{32} & 0 \end{pmatrix}. \tag{5}$$

Utilizing the time distribution T_{ij} from the state i to the state j, the state transition probability can be derived. Since there is only one event for the FBS moving away from state 3, we have $P_{32} = 1$. The event for the FBS exiting from state 2 is that the received signal energy strength whether satisfies the threshold level within the timer range T_0. Therefore, the transition probability P_{23} is

$$\begin{aligned} P_{23} &= \int_0^{\infty} m_{n_T}(t) P(T_{23} > t) dt \\ &= \int_0^{\infty} \lambda_m e^{-\lambda_m t} U(T_0 - t) dt = 1 - e^{-\lambda_m T_0}. \end{aligned} \tag{6}$$

Due to $P_{21} + P_{23} = 1$, then we have $P_{21} = 1 - P_{23} = e^{-\lambda_m T_0}$. Similarly, the event for the FBS exiting from the state 1 to state 2 is that the user initiates the session in the virtual cell coverage excluding the target FM coverage and the received signal energy strength meets the predefined threshold. Hence, the transition probability P_{12} can be obtained as

$$P_{12} = \frac{\lambda_c}{(\lambda_c + \lambda_m)} = 1 - \frac{\lambda_m}{\lambda_c}. \tag{7}$$

Due to $P_{12} + P_{13} = 1$, then we have $P_{13} = 1 - P_{12} = \lambda_m / \lambda_c$. From (3)–(7), we can derive the stationary probabilities given as follows:

$$\begin{aligned} \pi_1 &= \frac{P_{21}}{(2 + P_{21} P_{13})} = \frac{\lambda_c e^{-\lambda_m T_0}}{2\lambda_c + \lambda_m e^{-\lambda_m T_0}}, \\ \pi_2 &= \frac{1}{(2 + P_{21} P_{13})} = \frac{\lambda_c}{(2\lambda_c + \lambda_m e^{-\lambda_m T_0})}, \\ \pi_3 &= \frac{\lambda_m e^{-\lambda_m T_0} + \lambda_c \left(1 - e^{-\lambda_m T_0}\right)}{2\lambda_c + \lambda_m e^{-\lambda_m T_0}}. \end{aligned} \tag{8}$$

The mean residence time $\overline{t_1}$ and $\overline{t_2}$ can be easily derived as:

$$\overline{t_1} = \frac{1}{\lambda_c}, \tag{9}$$

$$\overline{t_2} = E[t_2] = E[\min\{T_{21}, T_{23}\}] = \frac{\left(1 - e^{-\lambda_m T_0}\right)}{\lambda_m}. \tag{10}$$

In state 3, the time duration is a busy period following $M/M/\infty$ queuing model, and thus the mean residence time $\overline{t_3}$ can be given by [17]

$$\overline{t_3} = \frac{\left(1 - e^{-\lambda_m / \rho}\right)}{\lambda_m}. \tag{11}$$

According to the stationary probability π_k and the mean residence time $\overline{t_k}$, the steady state probability P_k in each state can be obtained based on (3), and we have

$$\begin{aligned} P_1 &= \frac{\lambda_m e^{-\lambda_m T_0}}{2\lambda_m e^{-\lambda_m T_0} - \lambda_m e^{-\lambda_m (T_0 + 1/\rho)} + \lambda_c (1 - e^{-\lambda_m T_0})(1 - e^{-\lambda_m / \rho})}, \\ P_2 &= \frac{\lambda_c \left(1 - e^{-\lambda_m T_0}\right)}{2\lambda_m e^{-\lambda_m T_0} - \lambda_m e^{-\lambda_m (T_0 + 1/\rho)} + \lambda_c (1 - e^{-\lambda_m T_0})(2 - e^{-\lambda_m / \rho})}, \\ P_3 &= \frac{1 - e^{-\lambda_m / \rho}}{2 - e^{-\lambda_m / \rho}}. \end{aligned} \tag{12}$$

The partial derivative of the steady state probabilities with respect to the timer range T_0 are, respectively,

$$\frac{\partial P_1}{\partial T_0} = \frac{\lambda_m e^{-\lambda_m T_0}\left(e^{-\lambda_m T_0} - 1\right)}{\lambda_m e^{-\lambda_m T_0}\left(2 - e^{-\lambda_m/\rho}\right) + \lambda_c\left(1 - e^{-\lambda_m T_0}\right)\left(e^{-\lambda_m/\rho}\right)} < 0,$$

$$\frac{\partial P_2}{\partial T_0} = \frac{\lambda_m \lambda_c e^{-\lambda_m T_0}\left(2 - e^{-\lambda_m T_0}\right)}{\lambda_m e^{-\lambda_m T_0}\left(2 - e^{-\lambda_m/\rho}\right) + \lambda_c\left(1 - e^{-\lambda_m T_0}\right)\left(e^{-\lambda_m/\rho}\right)} > 0,$$

$$\frac{\partial P_3}{\partial T_0} = 0. \tag{13}$$

Therefore, the steady state probability P_1 and P_2 are the monotone decreasing function and the monotone increasing function with the increasing of T_0 respectively, while the steady state probability P_3 has nothing relationship with the timer range T_0. To simplify the description, we define:

$$f(\lambda_c, T_0) = 2\lambda_m e^{-\lambda_m T_0} - \lambda_m e^{-\lambda_m (T_0 + (1/\rho))} + \lambda_c\left(1 - e^{-\lambda_m T_0}\right)\left(2 - e^{-\lambda_m/\rho}\right). \tag{14}$$

In the subsequent, the analytic formulas of the energy consumption and average cumulative delay and interference time are expressed as:

$$E = \frac{\lambda_m e^{-\lambda_m T_0} E_1 + \lambda_c\left(1 - e^{-\lambda_m T_0}\right) E_2}{f(\lambda_m, \lambda_c, \rho, T_0)} + \frac{1 - e^{-\lambda_m/\rho}}{2 - e^{-\lambda_m/\rho}} E_3, \tag{15}$$

$$D_{\text{ave}} = \frac{\lambda_m^2 e^{-\lambda_m T_0}(D_{12} + D_{23}) + \lambda_c^2\left(1 - e^{-\lambda_m T_0}\right)^2 D_{23}}{\lambda_m^2 e^{-\lambda_m T_0} + \lambda_c^2 (1 - e^{-\lambda_m T_0})^2 + \lambda_c (1 - e^{-\lambda_m/\rho})^2 f(\lambda_m, \lambda_c, \rho, T_0)/(2 - e^{-\lambda_m/\rho})},$$

$$T_{\text{int}} = \frac{1 - e^{-\lambda_m/\rho}}{2 - e^{-\lambda_m/\rho}} T_H. \tag{16}$$

3.3. Analysis of the Compared Scheme. In this subsection, we analyze the existing prominent schemes theoretically and make a comparison among these schemes. IEEE 802.16 m [11] proposes a simple and practical scheme, called as periodical discontinuous transmission (PDTX), in which the FBS without active user changes alternately between available interval (AI) and unavailable interval (UAI). During the UAI, the FBS switches off the pilot transmission and the related processing. During the AI, the FBS becomes active on the air interface for synchronization and signaling purposes. In PDTX, Let τ be the low duty cycle in each period between AI and transmission period, the energy consumption and the cumulative interference time can be derived as

$$\begin{aligned} E_{\text{PDTX}} &= (1 - P_3)(1 - \tau)E_1 + (1 - P_3)\tau(E_3 - E_s) \\ &\quad + P_3(E_3 - E_s) \\ &= \tau(E_3 - E_1) + (1 - \tau)[P_3(E_3 - E_s - E_1) + E_1] \\ &= \tau(E_3 - E_1) + (1 - \tau) \\ &\quad \times \left[\frac{\left(1 - e^{-\lambda_m/\rho}\right)(1 - \tau)}{2 - e^{-\lambda_m/\rho}}(E_3 - E_s - E_1) + E_1\right], \end{aligned} \tag{17}$$

$$\begin{aligned} T_{\text{PDTX}} &= P_3 T_H + (1 - P_3)\tau T_H = [P_3(1 - \tau) + \tau] T_H \\ &= \left[\frac{\left(1 - e^{-\lambda_m/\rho}\right)(1 - \tau)}{2 - e^{-\lambda_m/\rho}} + \tau\right] T_H. \end{aligned} \tag{18}$$

Widiarti et al. [12] present a novel sleep mode for the FBS based on a grouping methodology, called as GPDTX. This scheme is closely related to the user location. The FBS in the absence of users switches off the pilot transmission, while the FBS with a nonactive user periodically transmit the pilot signal. Suppose that the user lies indoor with a probability P_{in}, and $P_{\text{out}} = 1 - P_{\text{in}}$. The energy consumption and the cumulative interference time can be derived as

$$\begin{aligned} E_{\text{GPDTX}} &= \left[\frac{P_{\text{in}}(1 - P_3)^2 \tau}{P_{\text{out}} + P_{\text{in}}(1 - P_3)} + P_3\right](E_3 - E_s) \\ &\quad + \left[\frac{P_{\text{in}}(1 - P_3)^2(1 - \tau)}{P_{\text{out}} + P_{\text{in}}(1 - P_3)} + \frac{P_{\text{out}}(1 - P_3)}{P_{\text{out}} + P_{\text{in}}(1 - P_3)}\right] E_1, \\ T_{\text{GPDTX}} &= \frac{P_{\text{in}}(1 - P_3)^2 \tau}{P_{\text{out}} + P_{\text{in}}(1 - P_3)} T_H + P_3 T_H. \end{aligned} \tag{19}$$

The partial derivatives of the energy consumption and interference time with respect to P_{in} are

$$\frac{\partial E_{\text{GPDTX}}}{\partial P_{\text{in}}} = \frac{(1 - P_3)^2 \tau (E_3 - E_s - E_1)}{(1 - P_3 P_{\text{in}})^2} > 0,$$

$$\frac{\partial T_{\text{GPDTX}}}{\partial P_{\text{in}}} = \frac{P_{\text{in}}(1 - P_3)^2 \tau}{(1 - P_3 P_{\text{in}})^2} T_H > 0. \tag{20}$$

Therefore, the energy consumption and cumulative interference time are the monotone increasing function with the increasing of P_{in}, respectively. It means the energy

efficiency of this scheme is directly relative to P_{in}. When $P_{\text{out}} = 0$, we have

$$E_{\text{GPDTX}} = [(1 - P_3)\tau + P_3](E_3 - E_s) + (1 - P_3)(1 - \tau)E_1, \quad (21)$$

$$T_{\text{GPDTX}} = (1 - P_3)\tau T_H + P_3 T_H. \quad (22)$$

Compare (17) and (21), (18) and (22), they are the same with each other. It implies that when the users stay at home all the time, GPDTX has the same energy-saving effect as PDTX. However, the signaling overhead of GPDTX is more serious than that of PDTX.

Reference [13] investigates the behavior of the sleep mode for the FBS based on user activity detection, called UDTX. The FBS switches off the pilot transmission until it detects the active user in its coverage. After completing the service for the active call, it immediately moves into a sleep mode. Hence, the energy consumption and interference time can be derived as

$$E_{\text{UDTX}} = (1 - P_3)E_1 + P_3 E_3 = E_1 + (E_3 - E_1)\frac{1 - e^{-\lambda_m/\rho}}{2 - e^{-\lambda_m/\rho}},$$
$$T_{\text{UDTX}} = P_3 T_H. \quad (23)$$

4. Performance Evaluation

In order to evaluate the performance of the proposed scheme, Monte Carlo simulation analysis is employed. A dual-strip model is chosen to simulate the multifloor based 3D femtocell cellular networks [15]. In this model, each stripe has 2 by 10 apartments and 6 floors. Each apartment is of size 10 m × 10 m. There is a street between the two stripes of apartments, with a width of 10 m. Each femto block is of 120 m × 70 m. Two critical parameters are introduced: the deployment rate ω and the activation rate ν. The deployment rate is used to simulate that each apartment has a FBS with a probability ω. The activation rate is defined as the active proportion of FBSs. If the FBS is active, it will transmit the user data in the traffic channel, or else it will transmit the pilot signal in the control channel. These two parameters determine operational femtocell density μ, that is, $\mu = \omega\nu$. Assume that femto users (FUEs) are randomly distributed on each floor of the building, and the session arrival of each FUE in the virtual cell coverage and the FM coverage follows Poisson distribution with the rate λ_c and λ_m.

The channel propagation model [15] includes path loss and log-normal shadowing. The path loss consists of free space loss, indoor path loss, indoor wall penetration loss, floor penetration loss, and outdoor wall penetration loss. If the FBS and the FUE (or another FBS) are inside the different apartments, the path loss is expressed as (24), or else (25). Consider

$$PL(\text{dB}) = \max\left(2.7 + 42.8\log_{10}R, 38.46 + 20\log_{10}R\right) + L_{ow,1} + 18.3 n_0^{((n_0+2)/(n_0+1)-0.46)} + q \times L_{iw} + L_{ow,2}0.7d_2, \quad (24)$$

$$PL(\text{dB}) = 38.46 + 20\log_{10}R + 0.7d_{2D,\text{indoor}} + 18.3\, n_0^{((n_0+2)/(n_0+1)-0.46)} + q \times L_{iw}, \quad (25)$$

where R denotes the distance between the FBS and the FUE (or another FBS), and $d_{2D,\text{indoor}}$ takes account of penetration loss due to walls inside an apartment. n_0 is the number of penetrated floors, q represents the number of walls separating apartments between the FBS and the FUE (or another FBS). L_{iw} is the penetration loss of the wall separating apartments, and $L_{ow,1}$ and $L_{ow,2}$ represent the penetration losses of outdoor wall for two houses, respectively.

Table 1: Simulation parameter.

Parameter	Value
System parameters	
Carrier frequency/bandwidth	2 GHz/10 MHz
Subcarrier bandwidth	15 kHz
Log-normal shadowing standard deviation	8 dB
Macrocell parameters	
Antenna pattern	Omni-directional
Macrocell radius	288 m
MBS height	32 m
Maximum MBS TX power	46 dBm
Femtocell parameters	
Maximum FBS TX power	20 dBm
User per femtocell	1
Deployment rate ω	80%
Activation rate ν	50%
Session arrival rate λ_m, $\lambda_c = 2\lambda_m$	5/h, 10/h, 20/h
The average service rate ρ	100/h

In addition, the simulation parameters are mostly referenced from [15] as summarized in Table 1. The simulation analysis is divided into the following two aspects. Firstly, with realistic LTE system parameters and 3D femtocell network model, we verify the rationality of the theoretical analysis and investigate the impact of the key parameters of the proposed scheme on the performance of femtocell networks. Secondly, we assess the effectiveness of the proposed scheme by comparing its performance with other three-prominent schemes.

4.1. Parameter Analysis of the Proposed Scheme. Figure 5 depicts steady state probability of the proposed scheme according to the timer range of the FBS. The close agreement between theoretical and numerical simulations indicates that analytic expressions (12) are the accurate approximations

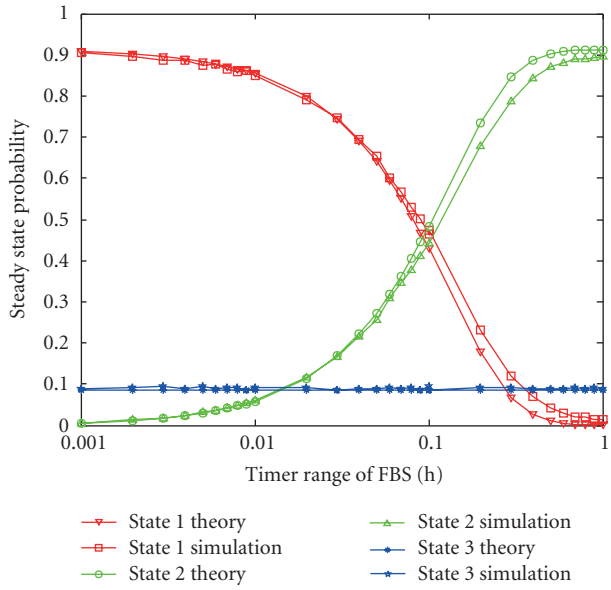

Figure 5: Steady state probability for both theory and simulation.

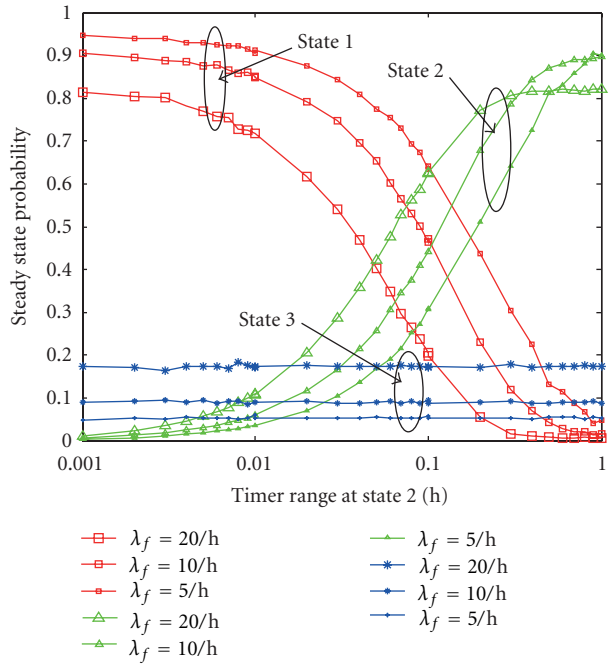

Figure 6: Steady state probability for numerical analysis.

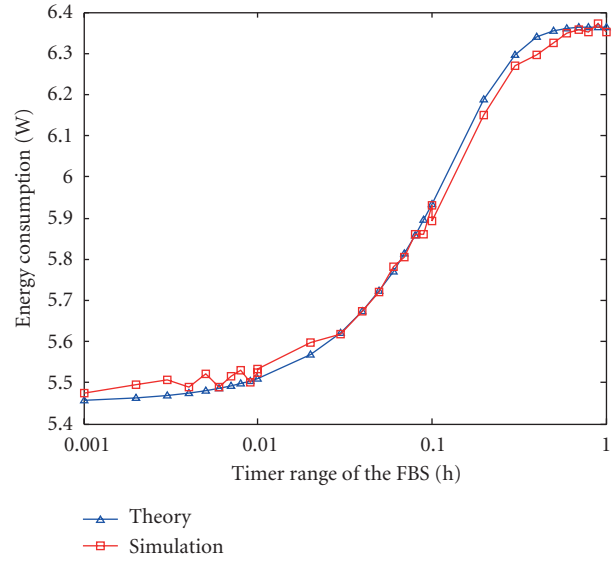

Figure 7: Energy consumption for both theory and simulation.

for practical steady state probability in the dense femtocell environments. Moreover, it can be seen that as the timer range of the FBS increases, the steady state probability of the state 1 decreases, the steady state probability of the state 2 increases, and the steady state probability of the state 3 has no correlation with the timer range and remains unchanged. That is also in accordance with the theoretical analysis.

Figure 6 shows the plots of the steady state probabilities of the proposed scheme from the simulation analysis. The steady state probabilities are compared with different session arrival rate. Moreover, for a fixed timer range of the FBS, as the session arrival rate increases, the steady state probability of state 1 decreases, while the steady state probabilities of both state 2 and state 3 increase. That is mainly due to the fact that the higher the session arrival rate, the greater the probability of the activation for the FM.

Figure 7 shows the energy consumption of the proposed scheme according to the timer range of the FBS. It can be seen that the theoretical analysis and numerical simulations get matched pretty well, which indicates that the analytic expression (15) is the accurate approximation for the practical energy consumption in dense femtocell environments. Moreover, we also can know that as the timer range of the FBS increases, the energy consumption increases. That is mainly due to the fact that the longer the timer range is, the greater the steady state probability of the state 3 is, which consumes the most energy of the all states.

Figure 8 depicts the relation between the energy consumption of simulation analysis and the timer range, respectively. For the same value of timer range, as the session arrival rate increases, the energy consumption increases. For fixed session arrival rate, the energy consumption increases with the increasing of the timer range.

Figure 9 depicts the average cumulative delay of the proposed scheme according to the timer range. It can be seen that as the timer range increases, the average cumulative delay decreases. That is mainly due to the fact that the greater the timer range, the more the session arrival will directly enter into the state 3, which will avoid the delay from state 1 to state 2. In addition, as the session arrival rate increases, the average cumulative delay decreases.

From the analysis above, we can conclude that the timer range has a significant effect on the energy consumption and the average cumulative delay and cumulative interference time. Hence, we should choose the proper timer range for the energy efficient FBS. Furthermore, as the timer range of

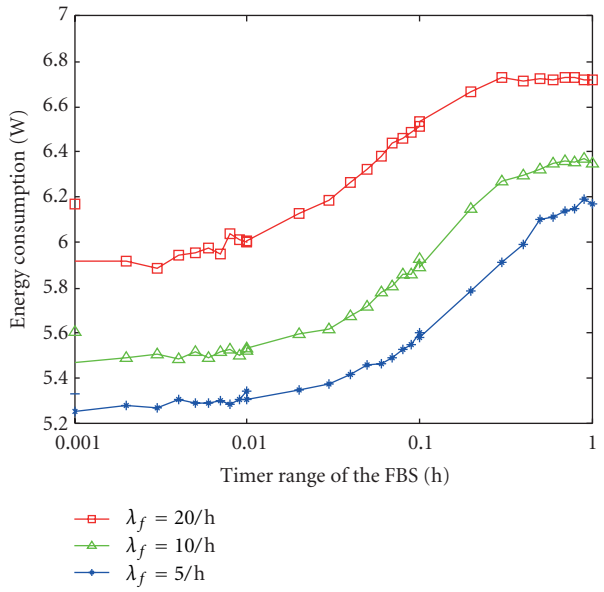

Figure 8: Energy consumption of simulation analysis versus timer range.

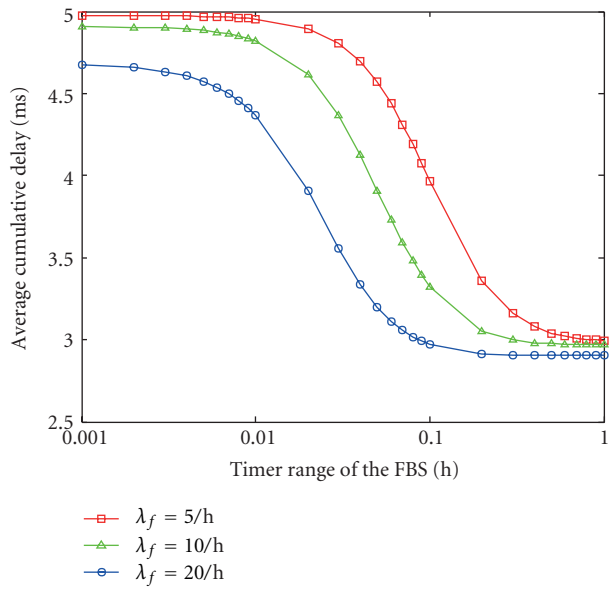

Figure 9: Average cumulative delay versus timer range.

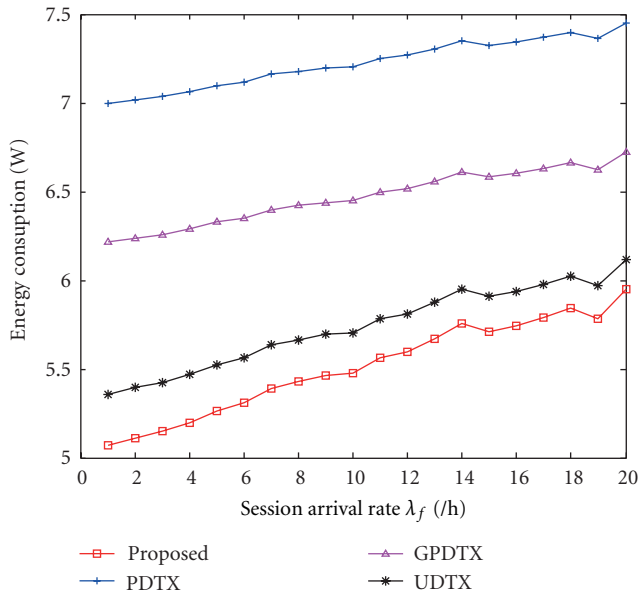

Figure 10: Energy consumption for different schemes.

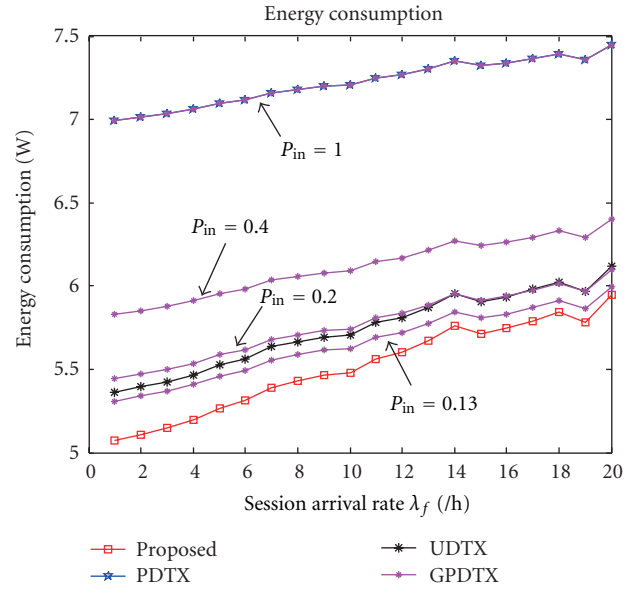

Figure 11: Energy consumption for different schemes with different P_{in}.

the FBS increases, curve trends of energy consumption and average cumulative delay are just contrary. Hence, we should elect the proper operation to balance them.

4.2. Performance Comparison with Different Schemes. Figure 10 and Figure 11 depict the energy consumption of different schemes with various session arrival rates. It is assumed that low duty cycle τ is 0.4 for two figures, and $P_{in} = 0.6$ for Figure 10. From these two figures, it can be seen that the energy consumption of all these schemes increases with the increasing of the session arrival rate. From Figure 10, for a fixed session arrival rate, the proposed scheme costs the lowest energy consumption of all schemes, while the traditional PDTX scheme spends the greatest energy consumption of all schemes. The energy consumption of femtocells using GPDTX is higher than using UDTX.

However, it can be seen from Figure 11 that the energy consumption of GPDTX decreases with the increasing of the probability P_{in}. When $P_{in} = 1$, the energy consumption curve of GPDTX is almost coincided with that of PDTX. When $P_{in} = 0.2$, the energy consumption curve of GPDTX is almost coincided with that of UDTX. When $P_{in} = 0.13$, the energy

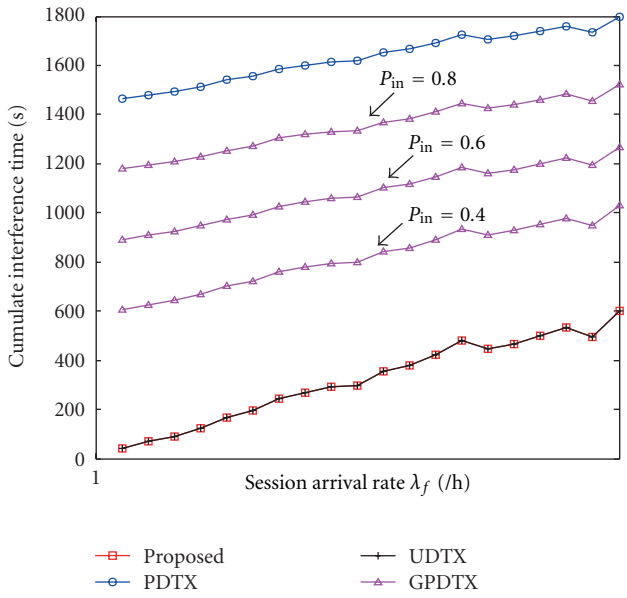

Figure 12: Interference time for different schemes with different P_{in}.

consumption of UDTX is higher than that of GPDTX. The reason is that when P_{in} is small, more FMs in the GPDTX scheme than in UDTX can completely switch off the pilot transmission due to the FBS grouping mechanism; when P_{in} is high, the UDTX scheme does not need to transmit the pilot signal with the nonactive user, but GPDTX scheme cannot do this. Finally, though our scheme is best in terms of the energy saving, it is achieved at the expense of more signaling overhead due to FBSs cooperation within each virtual cell.

Figure 12 shows the cumulative interference time for different scheme according to the session arrival rate. It can be seen that as the session arrival rate increases, the cumulative interference time for various schemes increase. For a fixed session arrival rate, the cumulative interference time using PDTX is the worst of all, while the curves of the proposed scheme and UDTX are nearly coincided with each other, and best of all. The cumulative interference time using GPDTX decreases with the decreasing of P_{in}.

5. Conclusion

This work proposes a novel hybrid BS-cooperative power management scheme for self-organized sleep mode in virtual cell-based femto networks. Firstly, according to the femtocell network topology, HBCPM builds a leader-member virtual cell framework. Within each virtual cell, the FBS is elected as either a FL or a FM based on the list degree and the sum of received pilot signal power. Moreover, because of the time variation characteristic of the femtocell network topology, the role assignment algorithm for the newly installed FBS is introduced. Secondly, the FL is responsible for detecting active calls in the virtual cell coverage, while the FMs in the absence of the active user can completely switch off the pilot transmission and the associated processing all the time. Thirdly, utilizing the semi-Markov process, state transition model of HBCPM is established, and then the analytic formulas of energy consumption and average cumulative delay and interference time are derived as well as three-prominent related schemes. Simulation results verify that the proposed scheme outperforms three existing schemes in terms of interference time and energy consumption. Further, the timer range of the proposed scheme has a significant effect on the energy consumption and the average delay.

In addition, this scheme can be easily applied to orthogonal frequency division multiple access (OFDMA) networks [18, 19], or orthogonal frequency and code division multiplexing (OFCDM) systems [20]. In the future, we plan to incorporate the user mobility model to study its effect on the performance of the proposed scheme and evaluate the energy consumption with the prominent related schemes. Further, we also plan to design and implement the FBS cooperative power management algorithm in official blocks.

Acknowledgments

This work is supported by the National S&T Major Project of China (no. 2010ZX03003-001-01, 2011ZX03003-002-01), and the Cobuilding Project of Beijing Municipal Education Commission, the National Natural Science Foundation of China (61101109), and the Youth Research and Innovation Project of Beijing University of Posts and Telecommunications.

References

[1] J. G. Andrews, H. Claussen, M. Dohler et al., "Femtocell past present and future," *IEEE Journal on Selected Areas in Communications*, vol. 30, pp. 497–508, 2012.

[2] W. C. Cheung, T. Q. S. Quek, and M. Kountouris, "Throughput optimization, spectrum allocation, and access control in two-tier femtocell networks," *IEEE Journal on Selected Areas in Communications*, vol. 30, pp. 561–574, 2012.

[3] J. H. Yun and K. G. Shin, "Adaptive interference management of OFDMA femtocells for co-channel deployment," *IEEE Journal on Selected Areas in Communications*, vol. 29, pp. 1225–1241, 2011.

[4] J. W. Huang and V. Krishnamurthy, "Cognitive base stations in LTE/3GPP femtocells: a correlated equilibrium game-theoretic approach," *IEEE Transactions on Communications*, vol. 59, pp. 3485–3493, 2011.

[5] S. Carlaw and C. Wheelock, "Femtocell market challenges and opportunities," *ABI Research, Research Report*, vol. 23, 2007.

[6] Z. Hasan, H. Boostanimehr, and V. K. Bhargava, "Green cellular networks: a survey, some research issues and challenges," *IEEE Communications Surveys & Tutorials*, vol. 13, pp. 524–540, 2011.

[7] C. Khirallah and J. S. Thompson, "Energy and cost impacts of relay and femtocell deployments in long-term-evolution advanced," *IET Communications*, vol. 5, pp. 2617–2628, 2011.

[8] W. Cheng, H. Zhang, L. Zhao, and Y. Li, "Energy efficient spectrum allocation for green radio in two-tier cellular networks," in *Proceedings of the 53rd IEEE Global Communications Conference (GLOBECOM '10)*, pp. 1–5, December 2010.

[9] A. D. Domenico, S. Emilio Calvanese, and D. Andrzej, "Ghost femtocells: an energy-efficient radio resource management

scheme for two-tier cellular networks," in *Proceedings of the 11th European Wireless Conference, Sustainable Wireless Technologies*, pp. 1–8, 2011.

[10] 3GPP, "TS36. 300 v11. 1. 0-E-UTRA and E-UTRAN Overall description Stage 2," 2012, http://www.3gpp.org/.

[11] IEEE P802.16m, "Part 16: Air Interface For Fixed And Mobile Broadband Wireless Access Systems-Advanced Air Interface," 2010.

[12] H. Widiarti, S. Y. Pyun, and D. H. Cho, "Interference mitigation based on femtocells grouping in low duty operation," in *Proceedings of the IEEE 72nd Vehicular Technology Conference Fall (VTC-Fall '10)*, pp. 1–5, September 2010.

[13] I. Ashraf, L. T. W. Ho, and H. Claussen, "Improving energy efficiency of femtocell base stations via user activity detection," in *Proceedings of the IEEE Wireless Communications and Networking Conference (WCNC '10)*, pp. 1–5, April 2010.

[14] 3GPP, "TS 22. 220 v11. 4. 0 Service requirements for Home Node B, (HNB) and Home eNode B, (HeNB)," 2011, http://www.3gpp.org/.

[15] 3GPP, "TR 36. 814 v9. 0. 0-Further advancements for E-UTRAN physical layer aspects," 2010, http://www.3gpp.org/.

[16] O. C. lbe, *Markov Processes for Stochastic Modeling*, Academic Press, 2009.

[17] D. Gross, J. F Shortle, J. M. Thompson, and C. M. Harris, *Fundamentals of Queueing Theory*, Wiley, 2008.

[18] H. Zhu and J. Wang, "Chunk-based resource allocation in OFDMA systems—part I: chunk allocation," *IEEE Transactions on Communications*, vol. 57, no. 9, pp. 2734–2744, 2009.

[19] Z. Huiling and W. Jiangzhou, "Chunk-based resource allocation in OFDMA systems—part II: joint chunk, power and bit allocation," *IEEE Transactions on Communications*, vol. 60, pp. 499–509, 2009.

[20] Y. Zhou, J. Wang, and M. Sawahashi, "Downlink transmission of broadband OFCDM systems—part I: hybrid detection," *IEEE Transactions on Communications*, vol. 53, no. 4, pp. 718–729, 2005.